

Water Resources Research

RESEARCH ARTICLE

10.1029/2018WR024615

Key Points:

- The topographic imprint of sand addition and bed flushing on water-worked gravel beds is analyzed using high-resolution photogrammetry
- Sand addition affects the roughness characteristics such as bed elevation standard deviation, skewness, and inclination index
- Bed flushing can clean the gravel bed surface from sand, with a return of roughness parameters to prepulse conditions

Supporting Information:

- Supporting Information S1

Correspondence to:

S. Bertin,
s.bertin@ymail.com

Citation:

Bertin, S., & Friedrich, H. (2019). Effects of sand addition and bed flushing on gravel bed surface microtopography and roughness. *Water Resources Research*, 55, 8076–8095. <https://doi.org/10.1029/2018WR024615>

Received 19 DEC 2018

Accepted 3 SEP 2019

Accepted article online 10 SEP 2019

Published online 15 OCT 2019

©2019. American Geophysical Union.
All Rights Reserved.

Effects of Sand Addition and Bed Flushing on Gravel Bed Surface Microtopography and Roughness

Stéphane Bertin^{1,2}  and Heide Friedrich¹ 

¹Department of Civil and Environmental Engineering, University of Auckland, Auckland, New Zealand, ²Now at Univ Brest, Institut Universitaire Européen de la Mer, Laboratoire Géosciences Océan UMR 6538, Plouzané, France

Abstract Gravel riverbeds naturally present a range of sediment size that can span several orders of magnitude. However, fine sediment (i.e., size <2 mm) additions affect sediment transport and are potentially harmful to the river ecology. Limited research has been done to understand the effects of sand addition on gravel bed topography. For this study, we conducted flume experiments testing the effectiveness of topography remote sensing to measure the response of a water-worked gravel bed to varying sand additions and bed flushing. Repeated measurements of the bed topography with through-water photogrammetry show that sand deposits primarily in low-lying areas of the bed, where it is sheltered. Observed changes in bed elevation standard deviation, skewness, and inclination index indicate a smoother bed, as sand fills the depressions on the surface and conceals gravel imbrication. The overall bed morphology (e.g., small bedforms and coarse grain arrangement), however, is preserved. Increasing the sand supply resulted in a gravel bed buried by sand and the formation of sand dunes. Bed flushing with a flow sufficient to move sand allowed a return of the bed roughness to the prepulse conditions, while flushing the bed with a discharge equivalent to the armoring discharge reworked the normally stable surface layer without removing infiltrated sand from the subsurface. This new data set contributes to providing missing information on the small-scale topographic effects of sand addition upon gravel beds. It might be used with measurements of near-bed flow hydraulics obtained in other studies to explain variations of sediment transport.

1. Introduction

The addition of fine sediment (i.e., sediment <2 mm) upon gravel bed surfaces can modify the appearance and properties of the bed considerably. Previous studies have reported effects ranging from fines filling gaps in the surface (Allan & Frostick, 1999; Beschta & Jackson, 1979; Frostick et al., 1984; Schälchli, 1992) to the complete blanketing of the bed (Gibson et al., 2011; Kuhnle et al., 2013; Wren et al., 2011), with various degrees in between, such as thin and patchy sand sheets over the coarser substrate (Ferguson et al., 1989; McLean, 1981; Wooster et al., 2008). Initially these processes have drawn the attention of the scientific community due to detrimental ecological effects in rivers. For instance, a reduction of reoxygenating intragravel flows and habitat degradation due to fine sediment infilling a gravel framework affect the survival rate of fish and other in-stream biota (Julien & Bergeron, 2006; Ryan, 1991; Zimmermann & Lapointe, 2005). Fine sediments also affect groundwater replenishment by reducing the bed permeability (Rosenberry & Healy, 2012; Schälchli, 1992), and they are known to provide anchorage for pollutants, such as heavy metals, radionuclides, and synthetic organic compounds (Krou et al., 2006; Macklin et al., 1997).

Processes associated with the delivery of fine sediment in a river are generally exacerbated as a result of an increase in fine sediment supply. Such increases may be natural, from relatively short-term or episodic events such as landslides, bank erosion, debris flows, and forest fires (Goode et al., 2012; Rickenmann, 1999; Sutherland et al., 2002). Anthropogenic disturbances can also result in large-scale sediment pulses through chronically accelerated erosion due to land use in the watershed (e.g., agriculture, forestry, and construction), gravel and other mining activities, and sediment release following dam removal and reservoir flushing (Downs et al., 2009; Kuhnle et al., 1996; Macklin et al., 1997; Roberts & Church, 1986). These fine sediment pulses, of varying magnitude and duration, not only affect the river ecology but also regulate the dynamics of sediment transport and thus the longer-term evolution and the forms of the river channels (Venditti et al., 2010a; Wilcock et al., 2001).

In this context, previous research interested in sand transport over a coarse bed explored the relations between sand supply limitation (e.g., due to the presence of an armor layer or limited supply from upstream) and the sand bedforms that can develop (Grams & Wilcock, 2014; Kleinhans et al., 2002; McLean, 1981; Tuijnder et al., 2009). Concerning the transport of the coarse bed fractions, the nature of the fine sediment is an important consideration as different sediments have been shown to affect the bed stability differently (Diplas & Parker, 1992; Perret et al., 2018). On one hand, silt and clay size material inhibits sediment transport by adding cohesion to the substrate (Barzilai et al., 2013). On the other hand, it is now well established that the addition of sand in gravel bed rivers can increase the gravel transport rate (Curran & Wilcock, 2005; Iseya & Ikeda, 1987; Jackson & Beschta, 1984). Although the exact mechanism is not completely understood, it has been associated to a reduction in the critical Shields stress for gravel entrainment (Wilcock et al., 2001). In particular, a grain size reduction at the bed and an increased transport capacity have been shown to counteract a tendency toward aggradation from an increased sediment supply (Curran & Wilcock, 2005; Dudill et al., 2018). Experiments show that not only sand, but sediment finer than the bed material, can be used to mobilize a coarse surface layer (Venditti et al., 2010a, 2010b). Because sand addition is detrimental to river ecology, the importance of this finding was put in the context of gravel augmentation, whereby finer gravel may be added to static gravel armors commonly found below dams, to unlock these beds in an attempt to rejuvenate salmon spawning gravels (Sklar et al., 2009).

Underlying mechanisms such as changes in the bed microtopography and roughness are generally invoked to explain the increased mobility of gravel after the addition of sand. Early work (reported in Venditti et al., 2010b) proposed that gravel transport increases due to some combination of hydraulic smoothing of the bed, reduction in the friction angle (the pivot angle a particle must rotate over to be entrained into transport), and a lack of disentrainment locations on the bed (Ikeda, 1984). Laboratory studies have confirmed that the addition of finer sediment causes systematic variations in channel hydraulics that can promote the mobilization process. In particular, measurements show an increase in the near-bed flow velocity (Venditti et al., 2010b; Wren et al., 2011), which was explained by finer sediment filling interstitial pockets and smoothing the bed. Experimental observations have also recognized that coarse sediment particles can wobble due to the flow and collisions with transported grains and that finer sediment falls in the spaces that were previously occupied (Dudill et al., 2017). As a consequence, coarse particles rest at a higher elevation, with an increased projection into the flow and a reduced friction angle, which both contribute to increase the probability of entrainment. Likewise, finer sediment can fill the dips and gaps created by entrained particles, removing potential disentrainment locations, so that once gravel is entrained, it does not come to rest again (Dudill et al., 2018).

In spite of this growing understanding, direct measurements documenting the key changes occurring at the gravel bed surface with the addition of fine sediment have not been obtained. Also, it remains unknown if these changes are reversible and if the bed structure returns to the prepulse conditions after the application of a competent flow of clear water, as it has been suggested previously (Detert & Parker, 2010; Kuhnle et al., 2016; Schälchli, 1992). Providing answers to these questions is necessary to substantiate past observations and has potentially important repercussions for research seeking to relate the changes in the small-scale topography of gravel bed rivers, due to the addition of fine sediment, to their effects on the larger river morphology and ecology. This study contributes to addressing this gap by demonstrating the effectiveness of, and applying, state-of-the-art topography remote sensing across three pilot experiments measuring the effects of sand addition and flushing on gravel bed microtopography and roughness. It was hypothesized that changes occurring at the gravel bed surface depend on the pulse morphodynamics and the initial bed topography, adopting different expressions in response to flow, sand quantity, and the degree of shelter upon the bed. We tested these hypotheses in a controlled flume environment using detailed measurements of gravel bed topography with through-water photogrammetry, while experimental parameters were systematically varied to form a range of testing conditions. We show that repeated high-resolution topography measurements provide meaningful information from which the effects of sand addition and surface flushing can be interpreted in terms of morphological changes (e.g., erosion and deposition) and measured using roughness parameters. These novel results are substantiated by a detailed analysis of the patterns of sand deposition and erosion, providing sedimentological explanations to the changes caused by the delivery and flushing of fine sediment upon gravel bed surfaces.

2. Experiments

2.1. Overview

Experiments were conducted in a 19-m-long, 0.45-m-wide, and 0.5-m-deep nonrecirculating tilting flume with glass side walls at The University of Auckland (Figure 1a). Gravel beds were prepared in a 1-m-long, 0.45-m-wide, and 0.13-m-deep sediment recess with a vertically adjustable table (called the test section) installed 10.4 m from the flume inlet. Natural gravel from the Tukituki River (Hawkes Bay, New Zealand) was used, with a distribution (Figure 1b) truncated at 2 and 35 mm (i.e., no sand present), a median grain size $D_{50} = 11.5$ mm, a sediment geometric sorting $\sigma_G = \sqrt{D_{84}/D_{16}} = 2.0$ and a specific gravity $SG = \rho_S/\rho_W = 2.6$ (where ρ_S and ρ_W are the density of sediment and water, respectively). The gravel was water-worked (conditions are explained below) to form a realistic and replicable bed arrangement before sand addition.

Fine sediment pulses consisted of coarse sand ($D_{50} = 0.9$ mm, $\sigma_G = 1.3$, and $SG = 2.6$) fed into the flume using a purpose-built apparatus. A plastic cylinder, with a sand capacity of 60 kg, was installed vertically above the flume centerline. A rectangular gap of adjustable size at the base of the cylinder allowed varying the feed rate q_{in} within a range of 0.055 to 4.07 kg/min (calibrated values). A small spinning motor with a decentered weight was attached to the feeding apparatus. Shaking enabled a constant feed rate throughout a test. A sloping plate with ridges and channels was mounted below the cylinder to spread the sand pulse across the flume width.

To facilitate the development of homogeneous hydraulic conditions in the flume and a fully turbulent boundary layer, the approach bed upstream of the test section was roughened by a fixed single-particle-thick layer of gravel, simulating the roughness of an armored bed by using only the coarsest fractions of the gravel mixture. The flume bed downstream of the test section was coated with a plastic mold of a stable armor obtained at the Leichtweiss-Institute for Hydraulic Engineering in Braunschweig, Germany (Spiller et al., 2012), with a surface texture and structure resembling the water-worked beds formed in our experiments. A similar arrangement was used to verify the replicability of stable gravel armors (Bertin & Friedrich, 2018); for the present work it also ensured more homogeneous sand transport compared to using a smooth bed.

In reporting the results of our experiment, three experimental runs (labeled Runs 3, 5, and 6) are presented. The three runs mimic different situations whereby fine sediment is introduced in a river. These ranged from a large magnitude short-lived event such as a landslide or reservoir flushing (Runs 5 and 6), to more moderate long-lasting sediment additions resulting, for example, from changes in land use in the catchment (Run 3). We note, however, that the pulses were by no means scaled to represent real events, as these are also variable. Rather, it was aimed to gain a general understanding of a gravel bed's response to pulses of variable magnitude and duration, as has been initiated by others before (e.g., Downs et al., 2009; Wooster et al., 2008). For each run, the slope (0.5%), grain size, and surface roughness of the gravel beds were virtually the same before sand addition, allowing comparison. Experimental conditions were then varied to assess the effect of key parameters, including testing different sand feed rates and hydraulic conditions during sand addition and subsequent bed flushing. The latter corresponds to the application of a clear flow of water in an attempt to clean the bed from sand. In addition to varying the parameters presented above, the effect of sand preconditioning of the bed (i.e., when the subsurface is already infiltrated by sand, a condition that may be more realistic of natural gravel beds) was examined by starting the tests either from clean (i.e., sand free) gravels (Runs 3 and 5) or from a gravel bed previously subjected to sand addition (Run 6).

Table 1 summarizes the experimental conditions used for the tests. For Runs 3 and 5 starting with a clean gravel bed, the well-mixed and sand-free gravel mixture was placed in the test section, screeded flat to a thickness of 0.13 m, parallel to the flume bed, and leveled with the surrounding fixed beds. The gravel bed was then armored at a constant flow discharge $Q = 90$ L/s (called the "armoring discharge," with a mean flow velocity $U = 0.81$ m/s and water depth $H = 0.245$ m) until the rate of sediment transport dropped to <1% of the initial value (armoring time ~ 100 hr). No sediment was fed during bed armoring, and the bed progressively degraded until a stable armor was formed. To keep the sediment bed leveled with the surrounding fixed beds, the sediment recess was manually adjusted upward with screw jacks according to the rate of erosion in the test section (Bertin & Friedrich, 2018). After armoring, the surface material was coarser than the bulk sediment (armor ratio ~ 1.5 , Figure 1b) and formed sedimentary

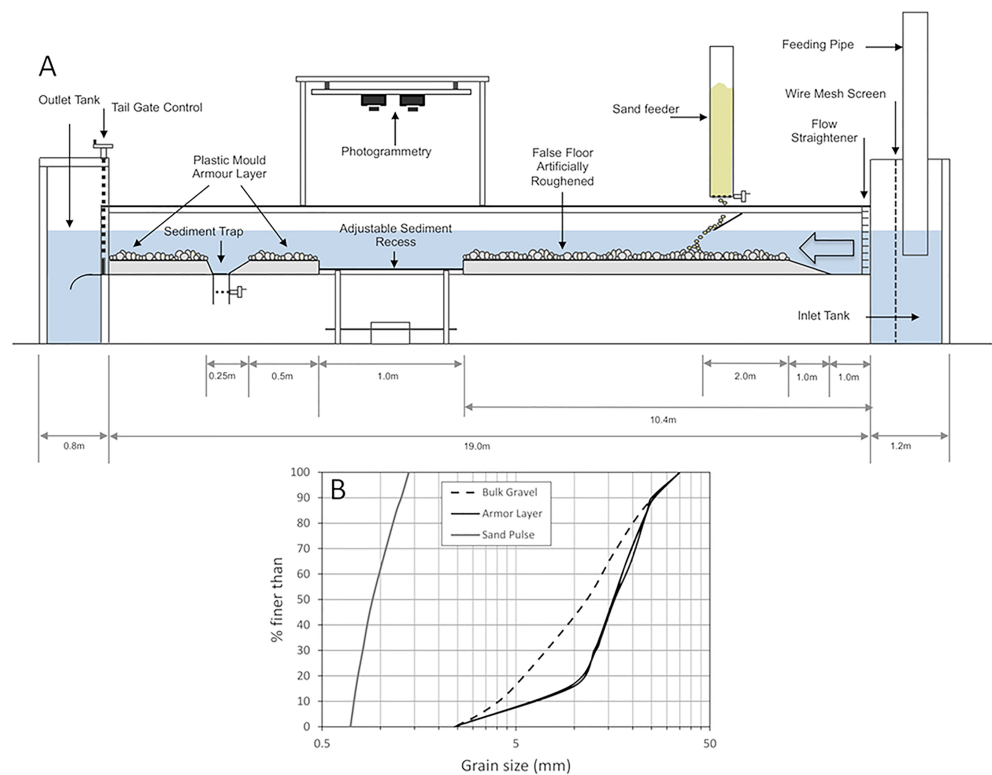


Figure 1. (a) Experimental setup and (b) grain size distributions (GSDs) of gravel (both bulk mixture and armor layer) and sand. GSDs for the bulk sediment mixtures were determined using size sieving corrected to account for the square holes (Church et al., 1987). GSD of the armor layer was determined for the three runs using Basegrain (Detert & Weitbrecht, 2012), calibrated to provide results comparable with weight-by-number GSDs (Stähly et al., 2017).

structures (e.g., grain imbrication, cluster microforms, and low-amplitude bed undulations) typical of natural gravel beds (Bertin et al., 2017). By applying the same forming conditions, this also enabled a replicable bed arrangement before sand addition (Bertin & Friedrich, 2018). Sand pulses were introduced 4 m from the channel entrance. For Run 3, two pulses of 40 kg each were added, while the flow discharge was reduced to $Q = 40$ L/s ($U = 0.53$ m/s, $H = 0.165$ m), a discharge only sufficient to move sand. To test the response of the bed to feed rate increases, sand feed rates (q_{in}) of 0.055 and 0.095 kg/min were used for the first and the second pulses, respectively. In any case, the feed rate was below the estimated sand transport capacity afforded by the flow, $q_{s*} = 0.4$ kg/min (cf. Table 1). Flushing the bed was done in two steps, with the flow initially continued at $Q = 40$ L/s, before it was increased to $Q = 90$ L/s (i.e., the armoring discharge). For all runs, bed flushing started after the pulse had completely traversed the flume and terminated when sediment transport became negligible. Runs 5 and 6 correspond to the largest feed rate used for the tests ($q_{in} = 4.07$ kg/min). For Run 5, the same hydraulic conditions as Run 3 were used, only sand feeding was different. In this case, the estimated transport capacity for sand was below the feed rate by a factor 10 (Table 1). For Run 6 starting with a gravel bed already infiltrated by sand, the bed obtained at the end of Run 5 served as initial bed condition. With a flow discharge $Q = 80$ L/s ($U = 0.76$ m/s and $H = 0.230$ m) during sand addition, the feed rate was approximately twice the estimated sand transport capacity. The flow was sufficient to entrain the loose gravel, but it was unable to break the gravel armor. The discharge was reduced to $Q = 40$ L/s for flushing the bed. Compared to keeping the flow rate steady during a test, changing the discharge among the three selected values for the experiment ($Q = 40$, 80, and 90 L/s) facilitated the efficient assessment of the effect of flow rate under more realistic conditions. This also enabled testing different flow sequences by changing the combination in which discharges are used.

Table 1
Pulse Characteristics and Hydraulic Conditions for Sand Addition and Bed Flushing Events

Initial bed	Sand feeding						Bed flushing							
	Pulse characteristics			Hydraulic conditions			Hydraulic conditions			Hydraulic conditions				
Run #	Pulse type	Mass (kg)	q_{in} (kg/min)	t^a (min; h)	Q (L/s)	Fr (-)	q_{s^*} (kg/min)	H (mm)	Flush type	Q (L/s)	Fr (-)	q_{s^*} (kg/min)	H (mm)	t^a (min; h)
3	Clean ^b	40	0.055	12 725	40	0.42	0.4	165	multiple	40	0.42	0.4	165	4,020 67
5	Clean ^b	40	4.07	7 10	40	0.42	0.4	165	single	90	0.52	2.6	245	1,440 24
6	Prefilled ^c	40	4.07	0.17 10	80	0.51	2.0	230	single	40	0.42	0.4	165	4,020 67

Note. Fr is Froude number calculated as U/\sqrt{gH} and q_{s^*} is the transport capacity for sand calculated using Van Rijn formulae accounting for both bedload (equation 12, van Rijn, 2007a) and suspended load (equation 17, van Rijn, 2007b).

^aDurations are expressed in both minutes and hours due to test runs and processes occurring over different time frames. Hydraulic conditions associated to sand feeding in Run 6 lasted 1 hr. This is shown in Figure 4c. ^bClean gravel bed corresponds to the gravel mixture free of sand. ^cPrefilled corresponds to the gravel mixture previously infiltrated by sand (here this corresponds to the final bed at the end of Run 5).

2.2. Measurements

During each run, we measured the pulse celerity, the sediment flux and composition, and the bed topography. A 0.2-m-long, full-width sediment trap with a 0.2-mm mesh, was installed 0.5 m downstream of the test section. After emptying the trap, the sediment was dried, sieved, and weighed to distinguish sand and gravel contributions to bedload. The pulse celerity was determined at 1-m intervals along the flume length by measuring the time at which the pulse first traversed each distance mark.

The evolution of bed topography at the test section was measured with digital photogrammetry. Detailed information on the camera setup and the workflow used for reconstructing digital elevation models (DEMs) is already presented elsewhere (e.g., Bertin et al., 2015), together with a validation of DEM quality using 3-D-printed ground truths. A brief overview is presented herewith. Two Nikon D5100 cameras (16.4 Mpixel, 23.6×15.6 mm² sensor size, 20-mm fixed focal lens) separated by 0.3 m were attached approximately 0.7 m above the flume centerline using a carriage, with both cameras looking down vertically at the bed, resulting in a ground pixel size ~ 0.15 mm. To obtain a high-resolution DEM of the test section (1×0.45 m², 1-mm grid spacing), three overlapping stereo images (i.e., six images in total) were collected. Each stereo image produced one DEM, after which the three DEMs were merged (Bertin et al., 2016) to obtain one DEM covering the full test section. To avoid draining and refilling the flume during a run, which can impact the bed topography, photos were taken after achieving a still water surface ($H = 0.13$ m) using the flume's tailgate. Through-water photogrammetry can produce high-quality results comparable with in-air measurements if refraction effects at the air-water interface are correctly accounted for (Dietrich, 2017), which was achieved in this study through calibration (Bertin et al., 2013). For quality assurance testing, DEMs were obtained both through water and in air at the end of each run. The point-to-point difference between DEMs was represented by a mean absolute error and a standard deviation of error (SDE) of 0.7 ± 0.1 and 1.1 ± 0.2 mm (i.e., $\mu \pm 1\sigma$, $n = 6$), respectively, which is comparable in quality to our previous studies (e.g., Bertin & Friedrich, 2018) and satisfied the conditions for reliable calculations from the DEMs.

Before analysis, DEMs were cropped to 850×350 mm² to minimize any flume wall effects, and elevations were normalized to have a zero mean bed level (i.e., $Z_{50} = 0$, where Z_{50} is the bed elevation for which 50% of the DEM elevations are smaller). DEMs were also detrended by fitting a flat surface by least squares to the raw elevation data, effectively removing the bed slope and photogrammetry setup misalignment (adding tilts to DEMs), which could otherwise conceal the topography of interest.

2.3. Analytical Methods

Roughness parameters calculated from the detrended DEMs are presented in Table 2. They are the bed elevation standard deviation σ_z , skewness S_K , kurtosis K_u , structure functions' horizontal roughness lengths in streamwise and cross-stream directions ($\Delta X0$ and $\Delta Y0$), and the inclination index in the flow direction $I0$. These surface metrics are calculated over the complete DEM size at different stages of the experiment to assess the effect of sand addition and flushing on bed roughness characteristics. Readers can refer to our previous work (Bertin & Friedrich, 2018; Groom et al., 2018) for detailed explanations of how roughness parameters are calculated. A brief presentation of their physical meaning is presented. Surface variability about the mean elevation within a DEM is indicated by σ_z , which can be used as a characteristic vertical roughness scale in flow

Table 2
Roughness Parameters Calculated From Detrended DEMs in This Study

Parameter	Formula
Standard deviation (σ_z)	$\sigma_z^2 = \frac{1}{N'} \sum_{i=1}^{N'} (Z_i - \langle Z_i \rangle)^2$
Skewness (S_k)	$S_k = \frac{1}{N' \sigma_z^3} \sum_{i=1}^{N'} (Z_i - \langle Z_i \rangle)^3$
Kurtosis (K_u)	$K_u = \left[\frac{1}{N' \sigma_z^4} \sum_{i=1}^{N'} (Z_i - \langle Z_i \rangle)^4 \right] - 3$
Structure function (D_{G2})	$D_{G2}(\Delta x, \Delta y) = \frac{1}{(N-n)(M-m)} \sum_{i=0}^{N-n} \sum_{j=0}^{M-m} \left\{ \left z(x_i + n\delta x, y_j + m\delta y) - z(x_i, y_j) \right \right\}^2$
Inclination index ($I0$)	$I0 = \frac{n_+ - n_-}{N_s}$

Note. z represents the bed elevation at location (x, y) in a DEM, N' is the total number of DEM points and $\langle \rangle$ represents the mean value. $\Delta x = n\delta x$ and $\Delta y = m\delta y$; δx and δy are the sampling intervals (i.e., DEM resolution) in the longitudinal and transverse directions, respectively; $n = 1, 2, 3, \dots, N$ and $m = 1, 2, 3, \dots, M$, where N and M are the number of DEM points in the same two directions. Following Nikora et al. (1998), horizontal roughness lengths in the streamwise ($\Delta X0$) and the cross-stream direction ($\Delta Y0$) were calculated from the 1-D second-order structure functions $D_{G2}(\Delta x, \Delta y = 0)$ and $D_{G2}(\Delta x = 0, \Delta y)$, respectively, and correspond to the spatial lags at which the tangent to the scaling region intercepts the saturation level. n_+ and n_- are the number of positive and negative slopes between successive DEM points, respectively, and N_s is the total number of slopes. Per convention, a positive slope refers to increasing bed elevations downstream. Following Millane et al. (2006), slopes whose absolute value is below 0.01 were deemed not reliable (i.e., neither positive nor negative) and were therefore not counted in the numerator. DEM = digital elevation model.

resistance equations. The degree of asymmetry of the elevation distribution is measured by S_k . For gravel beds, a positive skewness is indicative of a water-worked and armored surface and is attributed to finer grains filling depressions and reducing the magnitudes of surface deviations below mean bed level. K_u provides a measure of the regularity or intermittency of the bed. A distribution characterized by heavy tails and a narrow peak has a large kurtosis, with the variance due to infrequent extreme deviations. Uniform and compact distributions, of frequent modestly sized deviations from the mean, are of lower kurtosis values. $\Delta X0$ and $\Delta Y0$ are horizontal roughness scales calculated from bed elevation structure functions and are useful to determine the size of predominant bed features at the scale of interest. Finally, $I0$ measures the relative abundance of positive and negative slopes in the flow direction, which is indicative of grain imbrication (Millane et al., 2006).

Surface spatial variability at the grain scale was quantified for the different roughness parameters using a moving-window technique (Bertin et al., 2017). In light of our previous results this was done using windows with size equal to $5D_{50A}$ along both directions (i.e., square windows with axis length equal to 5 times the D_{50} of the bed surface material). Using the moving-window approach, roughness parameters are obtained for each window, while windows are moved across the DEM. An overlap between windows of 25% the window size was used, making for both efficient computations and reliable statistics as the number of windows fitting into the DEM neared 100.

To quantify the changes in bed microtopography resulting from sand addition and bed flushing, DEMs of differences (DoDs) were produced from DEMs collected at different epochs. Before subtraction, the DEMs were precisely aligned, both horizontally and vertically, using Matlab. The next step was to assess uncertainties in the DoDs and the calculation of a minimum level of detection (*minLOD*), which is critical to distinguish real topographic changes from the inherent noise or errors in measurements. Following the method presented in Brasington et al. (2003), *minLOD* was calculated as

$$\text{minLOD} = t \sqrt{(SDE_1)^2 + (SDE_2)^2} \quad (1)$$

where t is the confidence level (set to 1.28, representing a confidence interval [CI] of 80%) and SDE_1 and SDE_2 are the standard deviation of errors (here obtained by comparing through-water and in-air DEMs) for the two DEMs compared. For simplicity, and because SDE was consistent across runs (cf. section 2.2),

SDE = 1.1 mm was used throughout. This resulted in a *minLOD* of 1.99 mm. Consequently, when the difference in elevation in a given cell in absolute value is smaller than the *minLOD*, the change is not sufficient to be considered a real topographic change (e.g., deposition or erosion) given the measurement uncertainty and the confidence level and is omitted from the analysis. Hence, we measured volumetric changes between successive DEMs as the product of elevation change by cell area (1 mm²), using only those cells indicating sufficient change in regards to *minLOD*.

Geomorphic change detection using a *minLOD* is now applied extensively in river studies at the reach scale or higher (e.g., Brasington et al., 2003; Wheaton et al., 2010). To the best of our knowledge, it has not been used before on gravel patches. Here, using a CI of 80% promised reliable change detection. However, the resulting *minLOD* meant that change detection was essentially suited to small bedforms, gravel size particles, and sand sheets of thickness at least equivalent to three sand grain diameters ($D_{50,sand} = 0.9$ mm). The effects of *minLOD* on our ability to detect changes in sand content at the gravel bed surface and on the reliability of our observations made from a DoD were assessed in comparison with the results of an image analysis technique used as benchmark. The method adopted and the results are presented in the supporting information.

3. Experimental Observations

In this section we examine the expressions of sand accumulation and evacuation evidenced by our data set and methods, starting with the pulse morphodynamics. Interpretation of the findings and comparisons with other research are presented in section 4.

3.1. Pulse Transport

Differences in pulse transport and morphology were observed between runs. For Run 3, sand slowly dispersed downstream (Figure 2), without much sand accumulating at the point of introduction. Sand celerity was close to 0.1 m/min just after introduction and decreased to 0.06 m/min thereafter (Figure 2b). This resulted in a slight thickening of the sand pulse downstream, which in places could reach the gravels' top (Figure 3a). However, sand coverage remained patchy, comparable to sand sheets lightly draping areas of the bed in places, and with sand just able to fill the gaps between gravels otherwise. The second pulse in Run 3 had very similar effects to the first one in terms of the pulse transport and morphology (Figure 2), despite the feed rate being almost double (Table 1).

Sand transported faster in Runs 5 and 6, which used the largest feed rate in our experiments ($q_{in} = 4.07$ kg/min). A large sand accumulation (sand slug) formed at the point of introduction in the flume, eventually reaching 5 cm in height. Due to the constant addition of sand from upstream, the slug then grew longitudinally. For Run 6, which used a larger flow rate ($Q = 80$ L/s, compared to $Q = 40$ L/s in Runs 3 and 5), sand movement was also associated with grains that were picked up from the slug and rapidly dispersed downstream (forming the leading edge of the pulse). The celerity of the leading edge was faster than 5 m/min at the start, but it rapidly decreased and stabilized at around 0.8 m/min (Figure 2). The bulk of the pulse (i.e., the slug) transported more slowly, starting off with a celerity of around 1 m/min, which stabilized to around 0.5 m/min further downstream (Figure 2).

Visually, the effects of sand addition in Runs 5 and 6 were much more notable than in Run 3. The slug completely covered the surface with a layer of sand approximately 2–3 cm thick on average. After a short while, sand dunes formed on the bed, which disturbed the water surface and resulted in a drop in water elevation (~1–2 cm). The dune frontal geometry was typically 2-D, and dune propagation meant that regions of the bed in-between dunes were exposed to the flow (Figure 3b). For Run 6, gravel movement was observed as the dunes passed over the bed.

Sand cover thinned rapidly, starting from upstream, and those regions of the bed blanketed by sand were few and far between, as the sand addition was terminated. Supporting this observation, measured sediment fluxes (q_s) show that most of the sediment feed exited the flume relatively quickly after introduction (Figure 4). For Run 3, q_s returned to near zero 5 hr after the pulse ended. The large sand transport capacity ($q_s/q_{in} > 4$) meant that q_s (measured at the sediment trap located 8 m downstream of the point of introduction, causing a little lag in the response) aligned well with the feed rate (Figure 4a). For Runs 5 and 6, sand transport capacity was smaller than feed rate ($q_s/q_{in} \sim 0.1$ and ~ 0.5 for Run 5 and Run 6, respectively), which

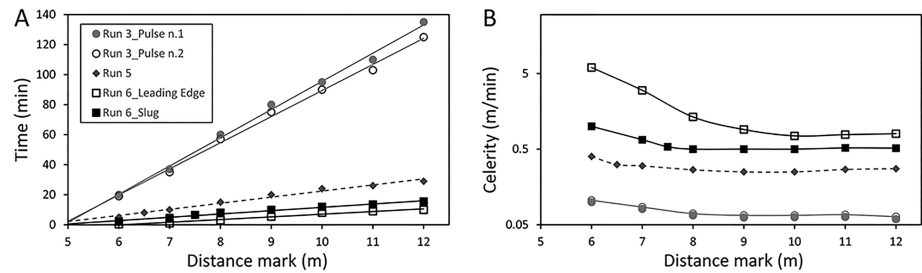


Figure 2. Pulse movement downstream (a) and pulse celerity (b) measured at 1-m intervals until the bedload trap. Linear relationships represent sand displacement very well ($R^2 > 0.95$), despite a decrease in pulse celerity with distance downstream. Time = 0 corresponds to fine sediment introduction. The zero-distance mark corresponds to the upstream end of the flume.

effectively capped sand transport in the flume (Figures 4b and 4c). Although, q_s peaked higher in Run 5, compared to Run 6, despite the higher flow velocity for Run 6. This can be explained by the dispersion of sand ahead of the slug in Run 6, which entrained a reduction in the peak transport rate as the slug reached the sediment trap.

3.2. Effect of Sand Addition on the Bed Topography
3.2.1. Run 3: Small Feed Rate, Long Duration, Low Flow

In the following, we assess how the different pulse morphodynamics observed in the experiment translated into different effects on bed microtopography and roughness. For Run 3, the first sand pulse filled the gaps between coarse grains and blanketed low-lying areas of the bed, effectively smoothing the bed (Figure 5b). Consequently, many of the small gravels initially visible on the armored bed (Figure 5a) were no longer distinguishable after sand addition. Instead, streaks of sand can be seen in the lee of a few coarse grains. They correspond to thicker deposits in the shadow zone behind gravels protruding high into the flow (Figure 5b). Outside of these relatively small geomorphic changes, comparing Figures 5a and 5b shows that the overall bed morphology, controlled by the arrangement of coarse grains and bedforms (e.g., humps and hollows), was unaffected by the sand pulse.

DoDs are presented in Figures 5c–5e. A minimum level of detection (*minLOD*) is used to filter out those supposed changes in bed topography that may in fact be the result of DEM errors. To evaluate the effect of *minLOD*, we varied the confidence level in the DoD using either 80% ($t = 1.28$) or 95% ($t = 1.96$) as the CI in equation (1), corresponding to a *minLOD* of 1.99 mm (Figure 5d) and 3.05 mm (Figure 5c), respectively. Using CI = 80%, it was found that sand deposited on 14% of the bed surface as a result of the first sand pulse (Figure 5d), while using CI = 95% indicated sand deposition over just 7% (Figure 5c). That is, only half of the deposits detected using CI = 80% were detected when CI = 95%. Comparison of our results with a benchmark provided by image analysis (cf. supporting information) confirmed the superiority of CI = 80% in that it improved the ability for detecting sand deposition, which was not counterbalanced by an increase in the

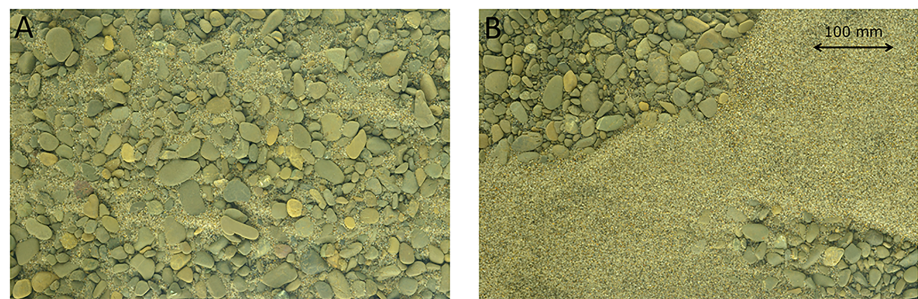


Figure 3. Contrasting photographs of the bed surface as the sand pulse traverses the test section during (a) Run 3 ($T = 12$ hr) and (b) Run 5 ($T = 0.5$ hr). Obtaining clear photographs through water ($H = 0.13$ m) required a still water surface, which was made possible by a significant decrease in flow discharge and raising the flume’s tailgate. Flow direction is from right to left.

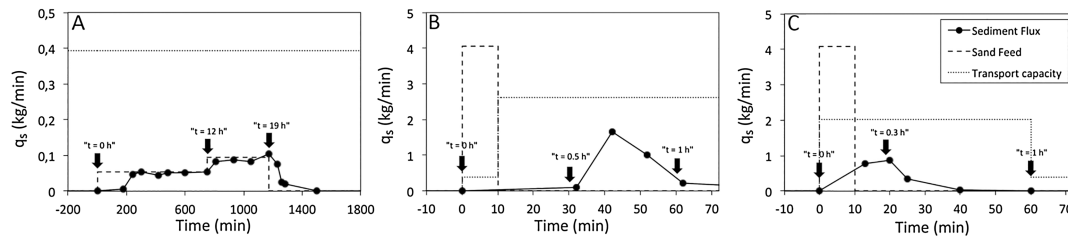


Figure 4. Bedload transport measured at the sediment trap (continuous line with markers), sand feed (dashed line), and sand transport capacity (dotted line) for (a) Run 3; (b) Run 5; and (c) Run 6. Arrows show the times at which bed topography was measured.

error rate (here the DoD cells wrongly indicating sand deposition). Using a CI below 80%, which we simulated by a reduction of *minLOD* below 1.99 mm, increased the error rate, potentially impacting the reliability of the results. For this reason, the analysis used $CI = 80\%$ for the remainder of the study, and hence only those topographic changes whose magnitude in absolute value was larger than $minLOD = 1.99$ mm are considered hereafter.

DoDs show that sand deposited preferably along what seems like two lines parallel to the flow direction, dividing the flume width (455 mm) into three almost equal parts (Figures 5d and 5e). Quite remarkably, little sand deposited near the flume centerline. Although we have no data to support this hypothesis, this may be the result of a nonuniform distribution of bed shear stress and the existence of secondary currents (McLean, 1981; Omran & Knight, 2010). During the first sand pulse (Figure 5d), deposition represented a volume of sand reaching 143 cm^3 (or 371 g). As volumes are evaluated as the product of DoD value by cell area after thresholding with *minLOD*, it cannot account for deposition in subsurface pores. Sand deposition was generally thin, with only 15% (areal) of the deposits thicker than 5 mm, and 50% thicker than 3 mm. Deposition occurred over 16% of the bed during the passage of the second pulse (Figure 5e), representing a total volume of 173 cm^3 (or 451 g). Two gravel particles were mobilized during the event (indicated in red in Figure 5e) and were transported over a short distance ($<150 \text{ mm}$). Both gravels were initially located above the mean bed level at an elevation of 4 mm (which corresponds to Z_{84}). Comparison of the DoDs (Figures 5d and 5e) shows that the regions of deposition after the passage of the first sand pulse persisted during the second pulse, with sand depositing at new locations and the thickness of the deposits increasing slightly.

In order to explain the mechanisms responsible for sand deposition (similar analysis is later applied to erosion), probability distribution functions (PDFs) of bed elevations were calculated for the regions of the initial bed (i.e., before sand addition) where sand deposition was detected after the passage of the pulse. For producing a PDF, regions identified as deposition (alternatively, erosion) in the DoD were “superposed” on the prepulse DEM to determine the elevation characteristics for those DEM cells only. This analysis shows that sand essentially covered regions of the gravel bed whose elevations were below the mean bed level before pulse (i.e., negative elevations). This is represented by a PDF’s mean elevation of -4.4 and -4.3 mm (corresponding to $\sim Z_{15}$ of the prepulse DEM) after the first and second pulses, respectively, and a negative distribution skewness for both. For the first pulse, only 10% of the regions of deposition had prepulse elevations above the mean bed level, which increased to 13% after the second pulse. Figure 5c shows that sand deposited at positive elevations in the case it could shelter behind a coarse grain protruding high into the flow. Accordingly, we observed a decreasing proportion of DoD cells indicating sand deposition with increasing bed elevations (Figure 5h). Low-lying regions of the gravel bed (for instance, with elevations below Z_{01}) were completely covered by sand after the passage of the pulse, which reduced to 50% for the regions with prepulse elevations corresponding to 7 mm or Z_{06} . In comparison, sand deposition was identified for only 7% of the DoD cells with a prepulse elevation equivalent to the mean bed level Z_{50} . A similar tendency was observed between the thickness of the sand deposits and the prepulse bed elevation, with thicker sand deposits generally covering low-lying regions of the bed and a decreasing sand thickness at higher bed elevations (Figure 5i).

3.2.2. Run 5: Large Feed Rate, Short Duration, Low Flow

The DEM for Run 5 at $T = 0.5$ hr shows irregular dunes over approximately half of the surface (Figure 6a), while the other half shows the exposed gravel bed with sand deposition limited to pockets between particles. Sixty-three percent of the bed represented in the DEM was covered by sand, corresponding to $3,184 \text{ cm}^3$ (or

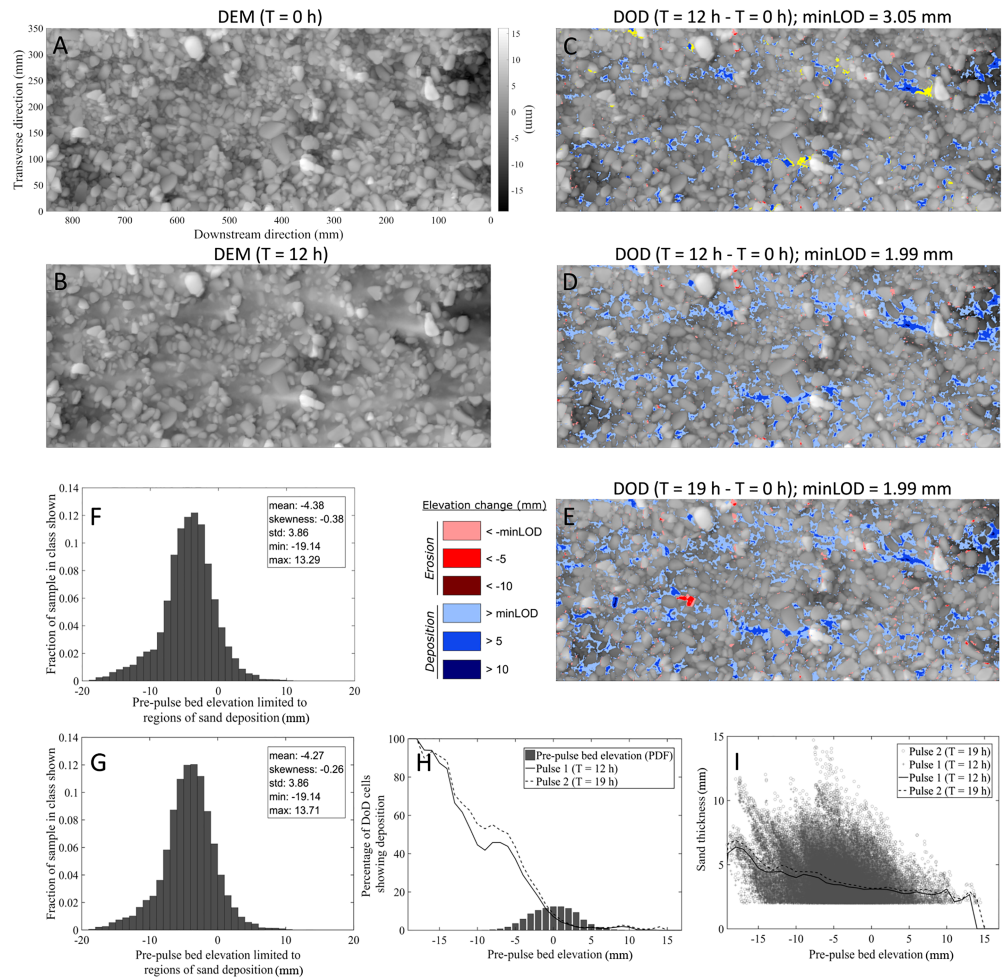


Figure 5. Repeat measurement of the bed topography during Run 3, showing (a) the DEM of the armored bed before sand addition ($T = 0$ hr); and (b) the DEM of the bed at the end of the first sand pulse ($T = 12$ hr). The DoD between (a, background image) and (b) was calculated using two confidence levels: (c) $t = 1.96$ corresponding to $CI = 95\%$ and $minLOD = 3.05$ mm; and (d) $t = 1.28$ corresponding to $CI = 80\%$ and $minLOD = 1.99$ mm. Regions of the DoD colored in yellow in (c) indicate where sand deposited above the mean bed level. The DoD (e) between the armored bed ($T = 0$ hr, background image) and the bed at the end of the second sand pulse ($T = 19$ hr) was calculated using $CI = 80\%$. Flow direction is from right to left, and vertical scaling is the same for all DEMs. Histograms (f, g) are the probability distribution functions of prepulse bed elevations at $T = 0$ hr for the cells identified as deposition at (f) $T = 12$ hr; and (g) $T = 19$ hr. (h) The percentage of DoD cells indicating deposition and (i) sand thickness after the passage of the sand pulses for different prepulse bed elevations. Sand thickness in (i) is presented as a scatter plot for all DoD cells indicating deposition and using line graphs for the average value. All dimensions are in millimeters. DEM = digital elevation model; DoD = DEM of differences.

8278 g). Because of the sand dunes, there is no relation between the locations where sand deposited and the underlying gravel bed elevations. Compared to Run 3, for which sand deposited mainly at low elevations, a more centered distribution with a mean elevation limited to regions of deposition of -0.63 mm (corresponding to Z_{42} of the prepulse DEM) was measured for Run 5 at $T = 0.5$ hr. The distribution skewness remained negative (skewness = -0.48), which is the result of sand depositing in the gaps between particles where the gravel bed was not covered by dunes.

At the time the pulse exited the flume ($T = 1$ hr, Figure 6b), the bed (and therefore the PDF of prepulse bed elevations for the regions of sand deposition) looked a lot more like what was observed during Run 3, with sand remaining in low-lying areas of the bed and behind coarse grains (PDF's mean elevation = -3.12 mm or Z_{22} and skewness = -0.38). At $T = 1$ hr, 20% of the bed remained covered by sand, corresponding to 198 cm^3 or 514 g.

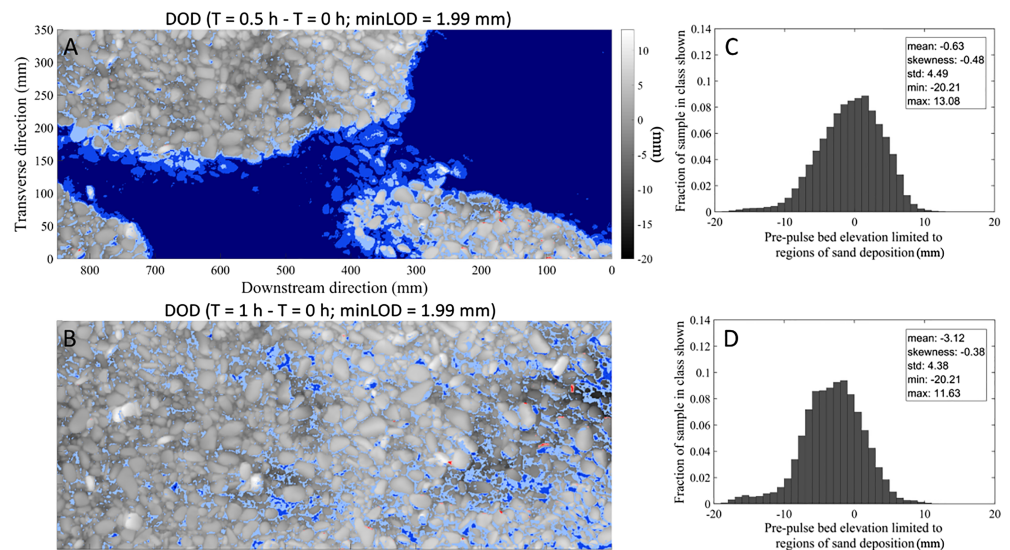


Figure 6. Repeat measurement of the bed topography during Run 5, showing the DoD between the armored bed before sand addition ($T = 0$ hr, background image) and (a) the bed during the passage of the sand pulse ($T = 0.5$ hr), and (b) the bed after the pulse completely exited the flume ($T = 1$ hr). The confidence level is $t = 1.28$ (i.e., CI = 80% and $\text{minLOD} = 1.99$ mm). Flow direction is from right to left, and vertical scaling is the same for all DEMs. Histograms (c, d) are the probability distribution functions of prepulse bed elevations at $T = 0$ hr for the cells identified as deposition at (c) $T = 0.5$ hr and (d) $T = 1$ hr. All dimensions are in millimeters. DEM = digital elevation model; DoD = DEM of differences.

3.2.3. Run 6: Large Feed Rate, Short Duration, High Flow

For Run 6, the sand pulse traversed the flume very quickly (Figure 2). Compared with Runs 3 and 5, the DoD ($T = 0.3$ hr, Figure 7a) shows both significant deposition and erosion. Deposition represents 13% of the DoD (i.e., $153 \text{ cm}^3/398 \text{ g}$) with erosion accounting for 4% (i.e., 52 cm^3 or 136 g). This corresponds to the net deposition of 101 cm^3 , or 262 g , of sediment. Similar to previous measurements barring the case where dunes were present on the bed, sediment (this time sand and gravel) deposited mostly at low elevations (mean elevation = -5.04 mm , i.e., Z_{15} of the prepulse DEM) although the bed elevation skewness was not negative this time. The particularity of Run 6 is the increased gravel transport, and we think that the change in skewness is also attributable to that. Especially as observations show that some of the transported gravels deposited after contact with a stable grain. They did not necessarily fall in pockets of the bed, which was different from the observations made for sand.

The PDF of prepulse bed elevations was also calculated for the regions of erosion. Unlike the PDFs for the regions of deposition, which show the elevations at which sediment grains came to rest (i.e., the pockets' elevation), the PDFs for the regions of erosion show the (particles') top elevation for the grains that were moved during the passage of the sand pulse. This presentation was preferred since the entrainment probability is often measured by the drag force, which is directly proportionate to the height of grain protrusion (e.g., Lamb et al., 2017). Our results show that essentially sediment grains whose tops were above the mean bed level were transported (PDF's mean elevation = 5.54 mm or Z_{90} and skewness = 0.15).

The bed was measured another time at $T = 1$ hr after the pulse introduction. The regions of sand deposition observed at $T = 0.3$ hr can no longer be seen, suggesting that continuing the flow after the pulse had traversed the test section effectively cleaned the sand from the bed surface. At $T = 1$ hr, regions of deposition and erosion both accounted for 8% of the bed surface. Although close to 0, the net volume change was for the first time negative ($-15 \text{ cm}^3/-38.7 \text{ g}$). Regions of (gravel) deposition were characterized by a mean elevation of -4.53 mm (Z_{18}) and a skewness of 0.09, which was similar to the observations made at $T = 0.3$ hr when the skewness was 0.06. This supports the observation made previously that gravels do not necessarily come to rest in pockets of the bed, which was a reason for the negative skewness in the case of sand. The PDF for erosion measured at $T = 1$ hr is similar to the PDF measured at $T = 0.3$ hr, showing that eroded grains mostly had a positive top elevation (mean elevation = 3.97 mm or Z_{78} , skewness = 0.07). However, the depth of

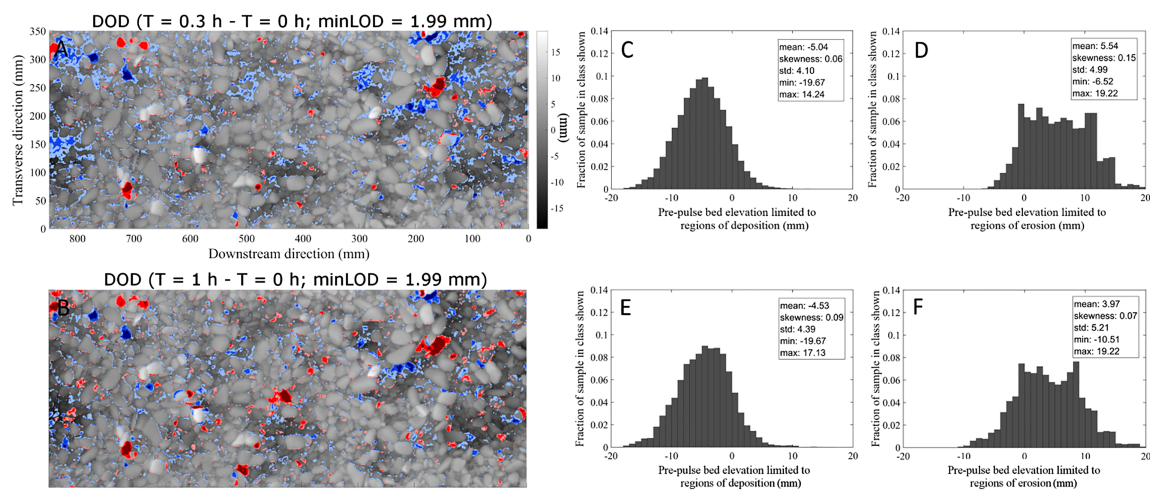


Figure 7. Repeat measurement of the bed topography during Run 6, showing the DoD between the armored bed before sand addition ($T = 0 \text{ hr}$, background image) and (a) the bed just after the passage of the sand pulse ($T = 0.3 \text{ hr}$), and (b) the bed after the pulse completely exited the flume ($T = 1 \text{ hr}$). The confidence level is $t = 1.28$ (i.e., $\text{CI} = 80\%$ and $\text{minLOD} = 1.99 \text{ mm}$). Flow direction is from right to left, and vertical scaling is the same for all DEMs. Histograms (c, d, e, f) are the probability distribution functions of prepulse bed elevations at $T = 0 \text{ hr}$ for the cells identified as deposition at (c) $T = 0.3 \text{ hr}$ and (e) $T = 1 \text{ hr}$, and the cells identified as erosion at (d) $T = 0.3 \text{ hr}$ and (f) $T = 1 \text{ hr}$. All dimensions are in millimeters. DEM = digital elevation model; DoD = DEM of differences.

erosion increased, which is indicated by the left tail of the PDF extending toward a new minimum elevation of -10.51 mm (compared to -6.52 mm at $T = 0.3 \text{ hr}$). A reason may be that the pulse smoothed the bed and loosened particles, which while initially stable were then more easily entrained as the flow was continued.

3.3. Effect of Bed Flushing on the Bed Topography

The effects of bed flushing identified in Runs 3 and 5 are analyzed in detail hereafter. For Run 6, flushing the bed at low flow ($Q = 40 \text{ L/s}$) did not impact the bed topography significantly with erosion concerning $\sim 1\%$ of the bed surface. Figure 7b showed previously that the bed had already undergone a cleaning of its sand during the continued application of high flow ($Q = 80 \text{ L/s}$ for 1 hr) after the pulse had traversed the test section. This left a quasi-static surface, and a flow rate reduction resulted in virtually no change.

For Run 3, continuing a low flow of $Q = 40 \text{ L/s}$ after sand feeding was terminated effectively removed most sand ($\sim 90\%$ by weight) from the bed surface. A comparison between the bed infiltrated by sand at $T = 19 \text{ hr}$ (i.e., the time at which sand addition was ended) and the prepulse armored bed ($T = 0 \text{ hr}$) previously indicated that 16% of the DEM surface was covered by sand, which was equivalent to 173 cm^3 or 451 g of sediment deposited in response to sand addition (Figure 5e). Now, comparing the DEMs preflushing and postflushing (Figure 8a) shows that erosion concerned 15% of the bed (i.e., $150 \text{ cm}^3/390 \text{ g}$). Using the DEM of the bed infiltrated by sand ($T = 19 \text{ hr}$) as reference shows that transport occurred mostly for sand grains with a top elevation just below the mean bed level (mean elevation = -1.41 mm or Z_{34} , skewness = -0.27), which corresponds on average to the top elevation of the sand deposits (Figure 5). Increasing the flushing flow to $Q = 90 \text{ L/s}$, which is the discharge used for preparing a static armor layer at the start of each run, further reshaped the bed due to the transport of gravels (Figure 8b), with erosion occurring over 12% of the surface ($170 \text{ cm}^3/441 \text{ g}$) and deposition 7% ($86 \text{ cm}^3/222 \text{ g}$). This resulted in a bed volume loss of 85 cm^3 or the erosion of 184 g of sediment (essentially gravel). Compared to bed flushing with $Q = 40 \text{ L/s}$, the mean elevation for regions of erosion increased (mean elevation = 0.17 mm or Z_{51}) but remained below the values observed for the erosion of gravel in Run 6 (Figure 7). The reason may be a difference in flow discharge between the two runs, whereby the higher flow rate of $Q = 90 \text{ L/s}$ used for bed flushing in Run 3 (compared to $Q = 80 \text{ L/s}$ in Run 6) could erode sediment grains deeper in the bed. However, the relatively small difference between the two flows suggests that this is only part of the explanation. What is readily observed in Figure 8b, when a gravel is flanked by blue on one side and red on the other side, is the indication that zones of erosion/deposition are in fact the result of gravels repositioning (not transport) with the flow. Those grains that could not be entrained but simply wobbled and rotated due to the flow are found at lower elevations

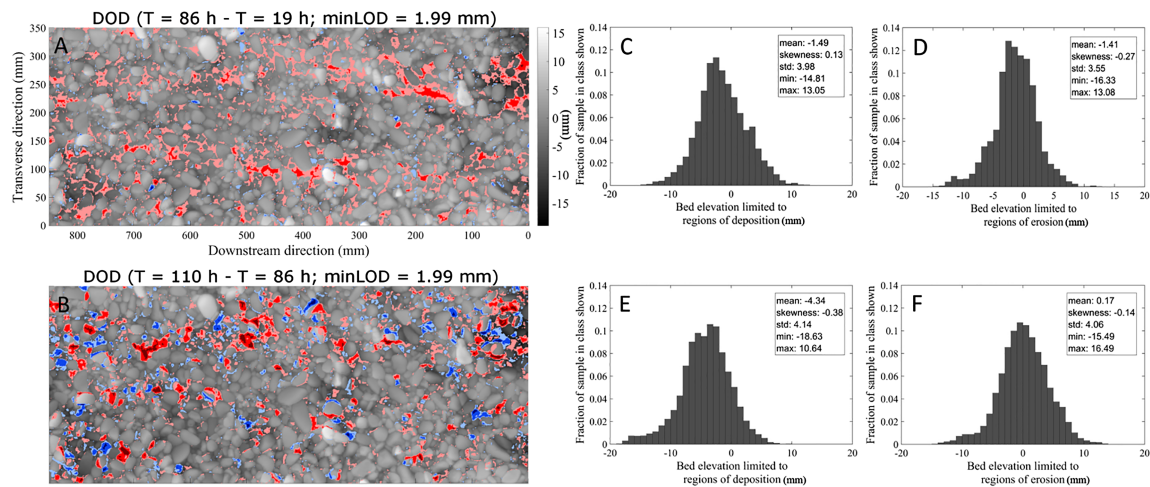


Figure 8. Repeat measurement of the bed topography during Run 3, showing (a) the DoD between the bed at the end of the second pulse ($T = 19$ hr, background image) and the bed after 67 hr of bed flushing with $Q = 40$ L/s ($T = 86$ hr); and (b) the DoD between the bed cleaned with $Q = 40$ L/s ($T = 86$ hr, background image) and the bed after 24 hr of bed flushing with $Q = 90$ L/s ($T = 110$ hr). The confidence level is $t = 1.28$ (i.e., CI = 80% and $minLOD = 1.99$ mm). Flow direction is from right to left, and vertical scaling is the same for all DEMs. Histograms (c, d) are the PDFs of preflushing bed elevations at the end of the second pulse ($T = 19$ hr) for the DEM cells identified as (c) deposition and (d) erosion at $T = 86$ hr, while histograms (e, f) are the probability distribution functions of bed elevations after bed flushing at $Q = 40$ L/s ($T = 86$ hr) for the cells identified as (c) deposition and (d) erosion at $T = 110$ hr. All dimensions are in millimeters. DEM = digital elevation model; DoD = DEM of differences.

than transported grains. Another reason would be the sand that was still present on the bed despite initial flushing at a discharge of 40 L/s. This sand was finally removed when high flow (90 L/s) was applied for bed flushing.

For Run 5 (Figure 9) directly applying a large flushing flow rate (90 L/s) on a bed with sand on the surface, erosion concerned 33% (536 cm³/1395 g), while deposition accounted for 10% (133 cm³/345 g). Before bed cleaning, sand covered 20% of the DEM (198 cm³/514 g, Figure 6b). Therefore, substantial gravel transport occurred as a result of bed flushing in Run 5. Visually, and also supported by the PDF, erosion picked up gravels reposing high on the bed, whereas sediment deposited at low elevations, such as troughs in the bed, and against the higher sediment forms.

3.4. Surface Roughness Adjustment

Previous sections have evaluated the effects of sand addition and flushing on the bed microtopography. In this section, morphological change is assessed in terms of surface roughness using a range of statistical analyses applied to the successive DEMs (Table 2).

A general observation for the three runs examined is a modification of the surface roughness as sand accumulates on the gravel bed and a return to prepulse conditions following bed flushing (Figure 10). There are some exceptions, which are discussed below. First, there are no significant changes ($p > 0.05$) in bed elevations' horizontal roughness lengths and kurtosis between the initial armored beds and the beds infiltrated by sand, suggesting that these parameters are not sensitive to the effects of sand addition. The effects of sand addition evidenced by our data are (i) a reduction of the bed elevation standard deviation, (ii) an increase in bed elevation skewness, and (iii) an inclination index measuring particle imbrication in a direction parallel to the flow becoming negative. This indicates a smoother bed due to sand, as sand fills the gaps between particles, and that particle imbrication characteristic of the armored surfaces (represented by a positive $I0$) is no longer identifiable. In particular, a negative $I0$ after sand addition indicates the predominance of negative slopes, which in this case is associated to sand deposition in the lee of gravels (cf. Figure 5b).

Observations for Run 5 generally differ from Runs 3 and 6. Especially at $T = 0.5$ hr, the bed elevation standard deviation and skewness were insensitive to sand addition when dunes occur, at least in terms of the medians, while horizontal roughness lengths responded with a significant increase (Figure 10). The latter could not be determined using moving windows, as the dunes extended beyond the window size (here,

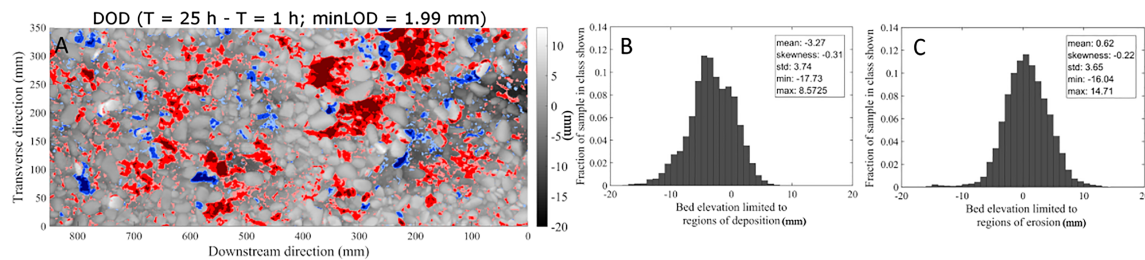


Figure 9. Repeat measurement of the bed topography during Run 5, showing (a) the DoD between the bed after the pulse completely exited the flume ($T = 1$ hr, background image) and the bed after 24 hr of bed flushing with $Q = 90$ L/s ($T = 25$ hr). The confidence level is $t = 1.28$ (i.e., CI = 80% and $minLOD = 1.99$ mm). Flow direction is from right to left. Histograms (b, c) are the PDFs of preflushing bed elevations after the pulse completely exited the flume ($T = 1$ hr) for the cells identified as (b) deposition and (c) erosion at $T = 25$ hr. All dimensions are in millimeters. DEM = digital elevation model; DoD = DEM of differences; PDF = probability distribution function.

$5D_{50A} \times 5D_{50A}$) and prevented the saturation region, that is, the spatial lag or distance at which bed elevations are not correlated anymore, to be attained. In this case, roughness lengths (e.g., ΔX_0) was measured over the entire DEM and reached 50.1 mm, which is considerably larger than ΔX_0 measured for the other runs where ΔX_0 was <15 mm. Run 5 also differed in terms of bed flushing. When a return to prepulse conditions was observed for Runs 3 and 6, σ_Z and ΔX_0 increased significantly following bed flushing for Run 5. We believe this is due to flushing at a high flow rate on a bed still covered by sand. We observed previously that significant bed erosion occurred in this case (Figure 9). Bed stability was restored at the condition a new armor layer developed. The latter was characterized by larger grain-scale morphological roughness (Figure 10).

In terms of spatial variability for the different roughness parameters, using a moving window shows that it did not vary in response to sand addition and bed flushing in that the interquartile range represented by the size of the boxes remained constant. The exception is the measurement of the bed topography at $T = 0.5$ hr in Run 5, which shows accentuated spatial variability in σ_Z due to the gravel bed being half covered by sand dunes.

4. Discussion

4.1. Assessment of Analysis Methods

Gravel bed surface adjustments resulting from sand addition and flushing have been examined in a controlled laboratory environment using repeated measurements of the bed topography in order to, first, quantify changes in the bed microtopography and roughness and, second, determine the patterns of sediment deposition and erosion that drive those changes. Surface roughness was assessed using a range of statistical parameters commonly used for gravel beds (e.g., Bertin & Friedrich, 2018; Smart et al., 2002), while subtracting successive DEMs to form a DoD provided an efficient and effective means to assess the magnitude and spatial extent of topographic changes (Brasington et al., 2003; Wheaton et al., 2010).

The ability to obtain high-resolution (1-mm grid spacing) and high-accuracy ($SDE = 1.1$ mm) DEMs through-water with photogrammetry, without the need to drain and refill the flume, warranted minimal external influence on the bed surfaces measured and an unprecedented level of geomorphic change detection from a DoD. However, despite the rigorous approach adopted to optimize DEM quality, and hence minimize errors in the DEMs (Bertin et al., 2015), residual measurement uncertainty eventually limited our ability to detect small geomorphic changes. The minimum level of detection ($minLOD$) in this study was estimated to be 1.99 mm.

The effect of $minLOD$ on measured sand accumulations was assessed using an image analysis technique as benchmark (cf. supporting information). The ability to accurately monitor sand patches on a gravel bed surface using image analysis was demonstrated by others previously, in the case of artificially colored sediment (e.g., Gibson et al., 2011; Sklar et al., 2009). For natural sediment, standard image analysis based solely on pixel intensity is not sufficient to automatically detect sand from gravel, due to similar colors. This required a purpose-built image analysis technique and manually coloring sand in photographs. This operation was extremely tedious and time consuming, which means that although acceptable for providing a control data set, image analysis could not be applied globally and at a large scale.

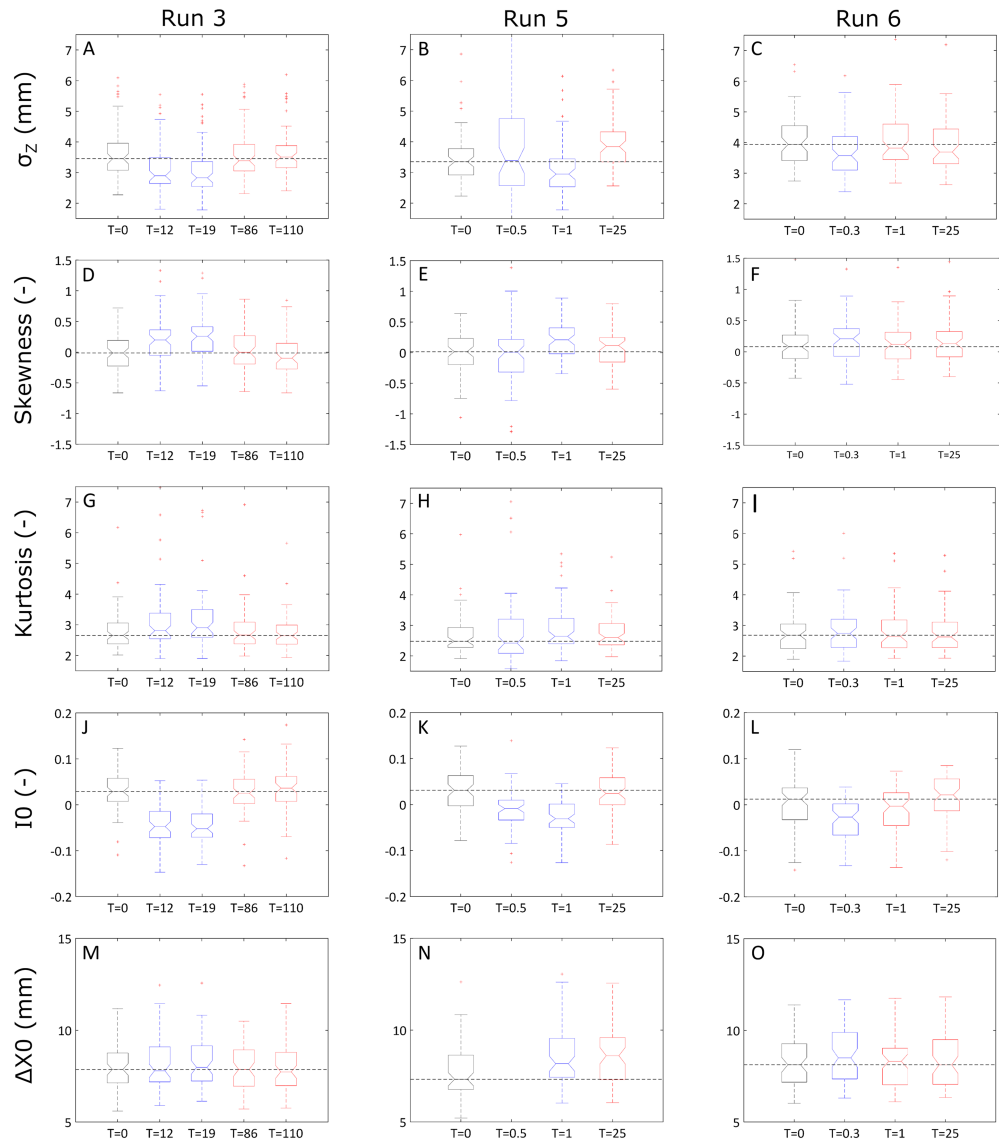


Figure 10. Evolution of surface roughness for Run 3 (a, d, g, j, m), Run 5 (b, e, h, k, n), and Run 6 (c, f, i, l, o). Boxes represent 25th–75th percentile range, notches indicate the interval for the median at a 95% confidence level, lines within boxes indicate median, lines above and below boxes show the range of extreme values which are not considered outliers (i.e., values within 1.5 of the interquartile range), and red crosses indicate outliers. Boxes are black for the armored beds before sand addition, blue for the beds infiltrated by sand, and red for the beds after flushing. The roughness parameters were calculated over square moving windows of size $5D_{50A} \times 5D_{50A}$ with a 25% overlap. The size of the moving windows prevented the measurement of $\Delta X0$ at $T = 0.5$ hr in Run 5. The graphs for $\Delta Y0$ are similar to those of $\Delta X0$ and thus are not presented. Dashed lines show the median value for the parameters before sand addition.

When image analysis results are compared with our topographic measurements it suggests that sand deposits with a thickness below *minLOD* may account for a significant proportion of all sand accumulations (up to 60% areal; Figures S2 and S3). These sand accumulations cannot be detected using topography remote sensing presently available. Despite these limitations, this study demonstrates that measuring bed topography can provide important new insights on the processes associated with sand addition and flushing in gravel bed rivers. Importantly, *minLOD* prevented the introduction of detection errors (e.g., DoD cells wrongly identified as deposition or erosion, Figure S3); this promised reliable observations made from DoDs and therefore guaranteed a high level of confidence for the findings.

Ongoing technological development (e.g., high-resolution cameras) will continue to improve our capability to detect small (approximately millimeters) geomorphic changes from DEMs. Other improvements may

result from applying more complex *minLOD* calculations, for example, methods harnessing the spatial coherence of sediment deposition and erosion (Wheaton et al., 2010). It is also imaginable that the effects of sand addition and flushing can be identified directly from bed surface photographs in future studies, at the condition that image analysis proves adequate to distinguish natural sand from gravel. Further work in this area would benefit field investigations for which the accurate measurement of submerged bed topographies remains challenging. In the laboratory, the improved ability to obtain both DEM and imagery data, for instance with the use of photogrammetric methods, means that the changes identified using image analysis can be mapped on the DEMs to determine their topographic signature.

4.2. Sand Pulse Effect on Bed Microtopography and Roughness

The range of flow conditions and feed rates used in the experiment meant that the sediment pulse adopted different expressions, from a thin and patchy sand sheet to a sand layer completely draping the gravel bed. These are believed to be representative of phenomena observed in nature, as it has been reported by others before (e.g., Frostick et al., 1984; Lisle, 1989, 2007). Although our ability to model the forms and processes associated with fine sediment addition and flushing was limited by the number of tests and the experimental design, varied conditions were used to showcase the wealth of information that can be derived from bed topographies. For the small feed rate with respect to the transport capacity (Run 3), sand was observed to infill pockets and drape low-lying areas of the bed, with higher deposits (sand streaks) forming in the lee of gravels protruding high into the flow. This effectively smoothed the bed, only minimally affecting coarse grain arrangement and bedform shape (e.g., the bed undulations formed with water-working). Large and short-lived sediment pulses (Runs 5 and 6) differed in that a sediment slug formed at the point of introduction, due to the flow not being able to carry the sand so quickly. The topographic expression of the slug evolved through distinct phases, which we summarize herewith. A thick layer of sand first covered the bed completely, transforming the initially coarse channel bed into a sand bed. As the front of the slug translated downstream, sand dunes formed and the bulk of transport was associated to dunes propagating. Upon terminating the addition of sand, the trailing edge of the slug started migrating downstream, leaving sections of the bed already traversed in a state resembling what was observed for a small feed rate, with sand lightly draping the surface and infilling bed pockets. The variations of sand bedform morphology observed in this study are consistent with previous research, which showed the occurrence of flow-parallel sand streaks (also called ribbons) under conditions of strong supply limitation and a smooth transition to dunes of increasing size and irregularity with decreasing supply limitation (Kleinhans et al., 2002; Tuijnder et al., 2009).

The topographic signature of the pulse barring the case when sand dunes cover the bed can be represented by a reduction in the bed elevation standard deviation and inclination index and an increase in bed elevation skewness, while kurtosis and horizontal roughness lengths did not change significantly due to the sand addition. Changes in the parameters aforementioned is in conformity with the visual smoothing of the bed and sand infilling bed pockets observed here and in other studies (e.g., Frostick et al., 1984; Kuhnle et al., 2013). Sand also filled the gaps between imbricated gravels and formed long deposits, thinning downstream in the shadow of protruding grains. Gravel imbrication was no longer identifiable after sand addition, with the inclination index adopting negative values (Figure 10). When sand dunes formed on the bed, the topographic expression of the pulse essentially manifested itself by a significant increase in horizontal roughness length, due to the large spatial extent of the dunes.

Previous studies measuring the effects of sand (or granule) addition on the flow hydraulics showed that infilling the pockets in a coarse surface layer resulted in near-bed velocity increases and reduced bed shear stress and turbulent fluctuations (Venditti et al., 2010b; Wren et al., 2011). It can be hypothesized that changes in near-bed flow properties can be related to variations of bed topography and surface roughness identified by our measurements. For instance, recent work proposed that the mean elevation of sand with respect to the gravel surface is an important parameter to explain the reduction in bed shear stress, with numerous practical applications. Grams and Wilcock (2007, 2014) developed a bed-sand coverage function to predict sand transport in suspension over a coarse immobile bed represented by hemispheres. Likewise, Kuhnle et al. (2013, 2016) presented relationships whereby the mean elevation of sand is used to predict sand transport and the cleanout depth for a given discharge. The relationships were derived from a series of flume experiments conducted over a manually screeded bed made of well-sorted gravel, with fine sand filling the bed from the bottom-up, which currently limits the applicability of the findings. The results presented

herewith (e.g., Figures 5–9) extend the range of conditions previously tested and maximizes the generality of the findings by using natural gravel water-worked to form a realistic surface before sand addition.

In spite of the recognition that changes in bed microtopography and roughness (e.g., different bed arrangements) are processes responsible for the increased mobility of gravel following sand addition, previous studies did not consider the bed topography exhaustively. Linking the changes in surface roughness to their effects on bedload transport was recently attempted by Barzilai et al. (2013) in the case where silt and clay-size material was introduced into an ephemeral river by a flash flood. Conversely to the mobilizing effect of sand, a gravel framework infilled by silt and clay is more resistant to entrainment, which in the case of the Nahal Eshtemoa (Israel) was represented by an increase in the critical shear stress to initiate bedload by a factor of 2 (Barzilai et al., 2013). Analysis of surface roughness was limited to the standard deviation of bed elevations, which showed a significant decrease when the gravel bed was infilled by fine sediment, indicating bed smoothing and a reduction in grain-scale morphological roughness. The same tendency observed in this study when sand is added to a water-worked gravel bed, however with contrasting effects on gravel transport, supports the conclusion that the cohesion imparted by silt and clay plays a predominant role in restraining sediment transport (Barzilai et al., 2013).

4.3. Can a Gravel Bed Return to Prepulse Conditions Following Bed Flushing?

The quantity of sand present on the coarse surface layer thinned rapidly after the passage of the pulse (Grams & Wilcock, 2007, 2014). This was indicated by a sediment flux returning to near 0 in a few hours after sand addition stopped. The reduction in sediment transport was even more rapid as the flow cleaning the bed was high (Figure 3). In this case, surface sand, even when protected in bed pockets and in the shadow behind coarse grains, was more easily entrained by the flow. This observation is in conformity with the theoretical work of Detert and Parker (2010) and the measurements carried out by Kuhnle et al. (2016), which showed that the depth of erosion for sand infiltrated into a gravel bed is proportional to the shear velocity at the bed.

Roughness parameters were observed to return to the conditions measured before sand addition, which supports our finding that most surficial sand was removed with bed flushing. When the effect of sand addition was a reduction in grain-scale morphological roughness, the opposite was observed during bed flushing with an increase in the standard deviation of bed elevations (σ_z) and inclination index ($I0$). In terms of modeling flow resistance using σ_z as a bed roughness parameter (Smart et al., 2002), our results imply that flow resistance effects operating on the bed (e.g., the partition between water depth and flow velocity) can be restored to the situation before sand addition through bed flushing.

Interestingly, flushing with the armoring discharge (i.e., 90 L/s) was observed to rework the normally stable armor layer in Run 5 but not in Run 3, which in the case of Run 5 resulted in a new armor layer with larger morphological roughness. For Run 3, a first cleaning of the bed at low flow ($Q = 40$ L/s) prior to application of the armoring discharge effectively removed most sand from the bed surface and restored roughness parameters (e.g., σ_z and $I0$) to their value before pulse (cf. Figure 10). In comparison, Run 5 used the armoring discharge directly on a bed with sand accumulations (Figure 6b) and a reduced surface roughness (Figure 10). The contrast between Run 3 and Run 5 suggests that sand content at the bed surface is an important control on bed stability, which was also identified by Perret et al. (2018). Another implication from our observations may be the possibility to use roughness parameters such as σ_z and $I0$ to assess changes in sand content at the surface of a gravel bed and to forecast the effect of bed flushing.

Subsurface processes differed from the observations made at the bed surface. Removing the sediment from the test section at the end of a run indicated that sand penetrated into the bed to an average distance equivalent to a few coarse grains diameter. This observation is in line with the results of numerous studies that can help to determine the propensity of fine sediment to infiltrate into a coarser framework and to describe the conditions in which this happens (e.g., Dudill et al., 2017; Gibson et al., 2010; Huston & Fox, 2015; Wooster et al., 2008). The volumes of sand removed from the test section after bed flushing amounted to ~ 1.9 kg ($\sigma = 0.13$ kg, $n = 5$), corresponding to $\sim 3\%$ by weight of the complete sediment mixture. No significant variation was observed between the different runs despite the range of conditions (e.g., volume of the pulse, flow hydraulics, and initial bed condition) used for the tests. In our experiments, the armoring discharge was the maximum discharge used for bed flushing. It would therefore be interesting to test the effect of bed flushing

with a discharge above the critical stability of the armored bed and the capability it has for cleaning the fines from the subsurface (called depth flushing; Wu & Chou, 2003). Although it was not tested directly, the experiments by Dudill et al. (2017, 2018) suggest that fine grains penetrate into a moving bed due to granular interactions via a process called kinetic sieving, suggesting that once fine sediment has infiltrated into a clean gravel bed, the composition of the latter appears to be permanently modified. For laboratory studies, this means that natural granular interactions occurring in moving beds may not be completely reproduced in a model when starting an experiment with a clean gravel bed. At lower flow velocities, such as in this study, we observed that sand in the subsurface does not play as important a role on surface processes as the sand present on the surface.

5. Conclusions

We presented a new laboratory data set testing and implementing topography remote sensing to study the effects of sand addition on gravel bed microtopography and roughness. Such measurements have not been obtained previously, despite it being frequently assumed that grain-scale modifications of the bed topography due to the inrush of fine sediment are responsible for changes in the overall bed morphology and ecology. Through bed flushing, we determined if the changes due to sand addition are reversible.

Repeated measurements of the bed topography were obtained with photogrammetry. This enabled geomorphic changes due to sand addition and bed flushing to be confidently determined by applying a minimum level of detection. Changes in surface roughness were analyzed using a range of parameters commonly used for gravel beds.

Our results confirm that the addition of sand on a water-worked gravel bed modifies the bed topography. We found that sand deposits mostly in low-lying areas of the bed. Fifty percent of the deposits had a thickness of less than 3 mm. Thicker deposits formed in the lee of coarse and protruding grains, even depositing sand above the mean bed level. In terms of surface roughness, the addition of sand had a notable effect on the bed elevation standard deviation, skewness, and the inclination index, but the effect on parameters like kurtosis and horizontal roughness lengths was not significant. Overall, these observations suggest a smoother bed after sand addition, with sand filling the depressions on the surface and concealing gravel imbrication, but the overall bed morphology (e.g., the bed undulations and coarse grain arrangement) remained unaffected. Increasing the sediment supply above the transport capacity afforded by the flow resulted in a gravel bed buried by sand and the formation of sand dunes. In this case, the bed should be considered as a sand bed, resulting in the presence of different transport mechanisms as compared to a gravel bed.

Sediment fluxes measured in the flume showed that most of the sand propagated as a pulse. Sand deposits thinned rapidly upon the supply termination. Bed flushing, with a flow sufficient to move sand, cleared the bed surface from the sand accumulated and allowed a return of the bed roughness to the prepulse conditions. Bed flushing with a discharge equivalent to the armor discharge reworked the normally stable surface layer, which was another proof that sand increases the transport capacity for gravel, and triggered an accentuated armor of the bed. However, excavating the beds indicated that sand remained in the pores below the surface layer, which could not be removed by bed flushing.

Discussion of our experimental results in association with previous research suggests that fine sediment addition to an initially clean gravel bed will impact the gradation of the bed permanently, due to fine sediment penetrating further into the bed during mobile bed conditions. More research is needed to address the connections between the changes in bed microtopography and roughness and the effect on near-bed hydraulics, as this may prove beneficial for our understanding of bedload transport for mixtures of gravel and sand. It is expected that continuous progress in topography remote sensing and image analysis techniques will benefit future studies interested in measuring the topographic signature of sand addition and bed flushing by easing current limitations related to the application of a minimum level of detection.

Acknowledgments

The data used in this paper are listed in the tables, figures, and supporting information. High-resolution DEMs are available online (from <https://water.auckland.ac.nz/data/>). The thoughtful comments of P. E. Grams and J. B. Laronne, along with those of the anonymous reviewers, helped to improve the manuscript and are greatly appreciated.

References

- Allan, A. F., & Frostick, L. E. (1999). Framework dilation, winnowing, and matrix particle size; the behavior of some sand-gravel mixtures in a laboratory flume. *Journal of Sedimentary Research*, 69(1), 21–26. <https://doi.org/10.2110/jsr.69.21>
- Barzilai, R., Laronne, J. B., & Reid, I. (2013). Effect of changes in fine-grained matrix on bedload sediment transport in a gravel-bed river. *Earth Surface Processes and Landforms*, 38(5), 441–448. <https://doi.org/10.1002/esp.3288>

- Bertin, S., & Friedrich, H. (2018). Effect of surface texture and structure on the development of stable fluvial armors. *Geomorphology*, 306, 64–79. <https://doi.org/10.1016/j.geomorph.2018.01.013>
- Bertin, S., Friedrich, H., & Delmas, P. (2016). A merging solution for close-range DEMs to optimize surface coverage and measurement resolution. *Photogrammetric Engineering and Remote Sensing*, 82(1), 31–40. <https://doi.org/10.14358/PERS.83.1.31>
- Bertin, S., Friedrich, H., Delmas, P., & Chan, E. (2013). *On the use of close-range digital stereo-photogrammetry to measure gravel-bed topography in a laboratory environment, 2013 LAHR Congress*. Chengdu, China: Tsinghua University Press.
- Bertin, S., Friedrich, H., Delmas, P., Chan, E., & Gimel'farb, G. (2015). Digital stereo photogrammetry for grain-scale monitoring of fluvial surfaces: Error evaluation and workflow optimisation. *ISPRS Journal of Photogrammetry and Remote Sensing*, 101, 193–208. <https://doi.org/10.1016/j.isprsjprs.2014.12.019>
- Bertin, S., Groom, J., & Friedrich, H. (2017). Isolating roughness scales of gravel-bed patches. *Water Resources Research*, 53, 6841–6856. <https://doi.org/10.1002/2016wr020205>
- Beschta, R. L., & Jackson, W. L. (1979). The intrusion of fine sediments into a stable gravel bed. *Journal of the Fisheries Research Board of Canada*, 36(2), 204–210. <https://doi.org/10.1139/f79-030>
- Brasington, J., Langham, J., & Rumsby, B. (2003). Methodological sensitivity of morphometric estimates of coarse fluvial sediment transport. *Geomorphology*, 53(3–4), 299–316. [https://doi.org/10.1016/S0169-555X\(02\)00320-3](https://doi.org/10.1016/S0169-555X(02)00320-3)
- Church, M. A., McLean, D. G., & Wolcott, J. F. (1987). *River bed gravel: Sampling and analysis*. Chichester: Wiley.
- Curran, J. C., & Wilcock, P. R. (2005). Effect of sand supply on transport rates in a gravel-bed channel. *Journal of Hydraulic Engineering*, 131(11), 961–967. [https://doi.org/10.1061/\(ASCE\)0733-9429\(2005\)131:11\(961\)](https://doi.org/10.1061/(ASCE)0733-9429(2005)131:11(961))
- Detert, M., & Parker, G. (2010). Estimation of the washout depth of fine sediments from a granular bed. *Journal of Hydraulic Engineering*, 136(10), 790–793. [https://doi.org/10.1061/\(ASCE\)HY.1943-7900.0000263](https://doi.org/10.1061/(ASCE)HY.1943-7900.0000263)
- Detert, M., & Weitbrecht, V. (2012). Automatic object detection to analyze the geometry of gravel grains, RiverFlow 2012, Taylor and Francis Group, San Jose, Costa Rica.
- Dietrich, J. T. (2017). Bathymetric structure-from-motion: Extracting shallow stream bathymetry from multi-view stereo photogrammetry. *Earth Surface Processes and Landforms*, 42(2), 355–364. <https://doi.org/10.1002/esp.4060>
- Diplas, P., & Parker, G. (1992). Deposition and removal of fines in gravel-bed streams. In P. Billi, R. D. Hey, C. R. Thorne, & P. Tacconi (Eds.), *Dynamics of gravel bed rivers* (pp. 313–329). Chichester, UK: Wiley & Sons.
- Downs, P. W., Cui, Y., Wooster, J. K., Dusterhoff, S. R., Booth, D. B., Dietrich, W. E., & Sklar, L. S. (2009). Managing reservoir sediment release in dam removal projects: An approach informed by physical and numerical modelling of non-cohesive sediment. *International Journal of River Basin Management*, 7(4), 433–452. <https://doi.org/10.1080/15715124.2009.9635401>
- Dudill, A., Frey, P., & Church, M. (2017). Infiltration of fine sediment into a coarse mobile bed: A phenomenological study. *Earth Surface Processes and Landforms*, 42(8), 1171–1185. <https://doi.org/10.1002/esp.4080>
- Dudill, A., Lafaye de Micheaux, H., Frey, P., & Church, M. (2018). Introducing finer grains into bedload: The transition to a new equilibrium. *Journal of Geophysical Research: Earth Surface*, 123, 2602–2619. <https://doi.org/10.1029/2018JF004847>
- Ferguson, R. I., Prestegard, K. L., & Ashworth, P. J. (1989). Influence of sand on hydraulics and gravel transport in a braided gravel bed river. *Water Resources Research*, 25(4), 635–643. <https://doi.org/10.1029/WR025i004p00635>
- Frostick, L. E., Lucas, P. M., & Reid, I. (1984). The infiltration of fine matrices into coarse-grained alluvial sediments and its implications for stratigraphical interpretation. *Journal of the Geological Society*, 141(6), 955–965. <https://doi.org/10.1144/gsjgs.141.6.0955>
- Gibson, S., Abraham, D., Heath, R., & Schoellhamer, D. (2010). Bridging process threshold for sediment infiltrating into a coarse substrate. *Journal of Geotechnical and Geoenvironmental Engineering*, 136(2), 402–406. [https://doi.org/10.1061/\(ASCE\)GT.1943-5606.0000219](https://doi.org/10.1061/(ASCE)GT.1943-5606.0000219)
- Gibson, S., Heath, R., Abraham, D., & Schoellhamer, D. (2011). Visualization and analysis of temporal trends of sand infiltration into a gravel bed. *Water Resources Research*, 47, W12601. <https://doi.org/10.1029/2011WR010486>
- Goode, J. R., Luce, C. H., & Buffington, J. M. (2012). Enhanced sediment delivery in a changing climate in semi-arid mountain basins: Implications for water resource management and aquatic habitat in the northern Rocky Mountains. *Geomorphology*, 139–140, 1–15. <https://doi.org/10.1016/j.geomorph.2011.06.021>
- Grams, P. E., & Wilcock, P. R. (2007). Equilibrium entrainment of fine sediment over a coarse immobile bed. *Water Resources Research*, 43, W10420. <https://doi.org/10.1029/2006WR005129>
- Grams, P. E., & Wilcock, P. R. (2014). Transport of fine sediment over a coarse, immobile river bed. *Journal of Geophysical Research: Earth Surface*, 119, 188–211. <https://doi.org/10.1002/2013jfe002925>
- Groom, J., Bertin, S., & Friedrich, H. (2018). Evaluation of DEM size and grid spacing for fluvial patch-scale roughness parameterisation. *Geomorphology*, 320, 98–110. <https://doi.org/10.1016/j.geomorph.2018.08.017>
- Huston, D. L., & Fox, J. F. (2015). Clogging of fine sediment within gravel substrates: Dimensional analysis and macroanalysis of experiments in hydraulic flumes. *Journal of Hydraulic Engineering*, 141(8), 04015015. [https://doi.org/10.1061/\(ASCE\)HY.1943-7900.0001015](https://doi.org/10.1061/(ASCE)HY.1943-7900.0001015)
- Ikeda, H. (1984). Flume experiments on the superior mobility of sediment mixtures. *Annual Report of the Institute of Geoscience*, 10, 53–56. Univ. of Tsukuba, Tsukuba, Japan
- Iseya, F., & Ikeda, H. (1987). Pulsations in bedload transport rates induced by a longitudinal sediment sorting: A flume study using sand and gravel mixtures. *Geografiska Annaler. Series A, Physical Geography*, 69(1), 15–27. <https://doi.org/10.2307/521363>
- Jackson, W. L., & Beschta, R. L. (1984). Influences of increased sand delivery on the morphology of sand and gravel channels. *JAWRA Journal of the American Water Resources Association*, 20(4), 527–533. <https://doi.org/10.1111/j.1752-1688.1984.tb02835.x>
- Julien, H. P., & Bergeron, N. E. (2006). Effect of fine sediment infiltration during the incubation period on Atlantic salmon (*Salmo salar*) embryo survival. *Hydrobiologia*, 563(1), 61–71. <https://doi.org/10.1007/s10750-005-1035-2>
- Kleinhans, M. G., Wilbers, A. W. E., De Swaaf, A., & Van Den Berg, J. H. (2002). Sediment supply-limited bedforms in sand-gravel bed rivers. *Journal of Sedimentary Research*, 72(5), 629–640. <https://doi.org/10.1306/030702720629>
- Krou, J. F., Fox, J. F., & Safferman, S. (2006). Experimental data and theoretical analysis of particle removal efficiency in a novel hydraulic separation unit. *Journal of Environmental Engineering*, 132(10), 1307–1313. [https://doi.org/10.1061/\(ASCE\)0733-9372\(2006\)132:10\(1307\)](https://doi.org/10.1061/(ASCE)0733-9372(2006)132:10(1307))
- Kuhnle, R. A., Bingner, R. L., Foster, G. R., & Grissinger, E. H. (1996). Effect of land use changes on sediment transport in Goodwin Creek. *Water Resources Research*, 32(10), 3189–3196. <https://doi.org/10.1029/96WR02104>
- Kuhnle, R. A., Wren, D. G., & Langendoen, E. J. (2016). Erosion of sand from a gravel bed. *Journal of Hydraulic Engineering*, 142(2). [https://doi.org/10.1061/\(ASCE\)HY.1943-7900.0001071](https://doi.org/10.1061/(ASCE)HY.1943-7900.0001071)
- Kuhnle, R. A., Wren, D. G., Langendoen, E. J., & Rigby, J. (2013). Sand transport over an immobile gravel substrate. *Journal of Hydraulic Engineering*, 139(2), 167–176. [https://doi.org/10.1061/\(ASCE\)HY.1943-7900.0000615](https://doi.org/10.1061/(ASCE)HY.1943-7900.0000615)
- Lamb, M. P., Brun, F., & Fuller, B. M. (2017). Direct measurements of lift and drag on shallowly submerged cobbles in steep streams: Implications for flow resistance and sediment transport. *Water Resources Research*, 53, 7607–7629. <https://doi.org/10.1002/2017wr020883>

- Lisle, T. E. (1989). Sediment transport and resulting deposition in spawning gravels, north coastal California. *Water Resources Research*, 25(6), 1303–1319. <https://doi.org/10.1029/WR025i006p01303>
- Lisle, T. E. (2007). The evolution of sediment waves influenced by varying transport capacity in heterogeneous rivers. In H. P. H. Habersack, & M. Rinaldi (Eds.), *Gravel-bed rivers VI: From process understanding to river restoration* (Vol. 11, pp. 443–469), Amsterdam, Netherlands. [https://doi.org/10.1016/S0928-2025\(07\)11136-6](https://doi.org/10.1016/S0928-2025(07)11136-6)
- Macklin, M. G., Hudson-Edwards, K. A., & Dawson, E. J. (1997). The significance of pollution from historic metal mining in the Pennine orefields on river sediment contaminant fluxes to the North Sea. *Science of The Total Environment*, 194-195, 391–397. [https://doi.org/10.1016/S0048-9697\(96\)05378-8](https://doi.org/10.1016/S0048-9697(96)05378-8)
- McLean, S. R. (1981). The role of non-uniform roughness in the formation of sand ribbons. *Marine Geology*, 42(1-4), 49–74. [https://doi.org/10.1016/0025-3227\(81\)90158-4](https://doi.org/10.1016/0025-3227(81)90158-4)
- Millane, R. P., Weir, M. I., & Smart, G. M. (2006). Automated analysis of imbrication and flow direction in alluvial sediments using laser-scan data. *Journal of Sedimentary Research*, 76(8), 1049–1055. <https://doi.org/10.2110/jsr.2006.098>
- Nikora, V. I., Goring, D. G., & Biggs, B. J. F. (1998). On gravel-bed roughness characterization. *Water Resources Research*, 34(3), 517–527. <https://doi.org/10.1029/97WR02886>
- Omran, M., & Knight, D. W. (2010). Modelling secondary cells and sediment transport in rectangular channels. *Journal of Hydraulic Research*, 48(2), 205–212. <https://doi.org/10.1080/00221681003726288>
- Perret, E., Berni, C., Camenen, B., Herrero, A., & Abderrezzak, K. E. K. (2018). Transport of moderately sorted gravel at low bed shear stresses: The role of fine sediment infiltration. *Earth Surface Processes and Landforms*, 43(7), 1416–1430. <https://doi.org/10.1002/esp.4322>
- Rickenmann, D. (1999). Empirical relationships for debris flows. *Natural Hazards*, 19(1), 47–77. <https://doi.org/10.1023/a:1008064220727>
- Roberts, R. G., & Church, M. (1986). The sediment budget in severely disturbed watersheds, Queen Charlotte Ranges, British Columbia. *Canadian Journal of Forest Research*, 16(5), 1092–1106. <https://doi.org/10.1139/x86-189>
- Rosenberry, D. O., & Healy, R. W. (2012). Influence of a thin veneer of low-hydraulic-conductivity sediment on modelled exchange between river water and groundwater in response to induced infiltration. *Hydrological Processes*, 26(4), 544–557. <https://doi.org/10.1002/hyp.8153>
- Ryan, P. A. (1991). Environmental effects of sediment on New Zealand streams: A review. *New Zealand Journal of Marine and Freshwater Research*, 25(2), 207–221. <https://doi.org/10.1080/00288330.1991.9516472>
- Schälchli, U. (1992). The clogging of coarse gravel river beds by fine sediment. *Hydrobiologia*, 235-236(1), 189–197. <https://doi.org/10.1007/bf00026211>
- Sklar, L. S., Fadde, J., Venditti, J. G., Nelson, P., Wyzdga, M. A., Cui, Y., & Dietrich, W. E. (2009). Translation and dispersion of sediment pulses in flume experiments simulating gravel augmentation below dams. *Water Resources Research*, 45, W08439. <https://doi.org/10.1029/2008WR007346>
- Smart, G., Duncan, M., & Walsh, J. (2002). Relatively rough flow resistance equations. *Journal of Hydraulic Engineering*, 128(6), 568–578. [https://doi.org/10.1061/\(ASCE\)0733-9429\(2002\)128:6\(568\)](https://doi.org/10.1061/(ASCE)0733-9429(2002)128:6(568))
- Spiller, S., Rütger, N., & Baumann, B. (2012). Artificial reproduction of the surface structure in a gravel bed, 2nd IAHR Europe Congress, TU München, Germany.
- Stähly, S., Friedrich, H., & Detert, M. (2017). Size ratio of fluvial grains' intermediate axes assessed by image processing and square-hole sieving. *Journal of Hydraulic Engineering*, 143(6). [https://doi.org/10.1061/\(ASCE\)HY.1943-7900.0001286](https://doi.org/10.1061/(ASCE)HY.1943-7900.0001286)
- Sutherland, D. G., Ball, M. H., Hilton, S. J., & Lisle, T. E. (2002). Evolution of a landslide-induced sediment wave in the Navarro River, California. *GSA Bulletin*, 114(8), 1036–1048. [https://doi.org/10.1130/0016-7606\(2002\)](https://doi.org/10.1130/0016-7606(2002))
- Tuijinder, A. P., Ribberink, J. S., & Hulscher, S. J. M. H. (2009). An experimental study into the geometry of supply-limited dunes. *Sedimentology*, 56(6), 1713–1727. <https://doi.org/10.1111/j.1365-3091.2009.01054.x>
- van Rijn, L. C. (2007a). Unified view of sediment transport by currents and waves. I: Initiation of motion, bed roughness, and bed-load transport. *Journal of Hydraulic Engineering*, 133(6), 649–667. [https://doi.org/10.1061/\(ASCE\)0733-9429\(2007\)133:6\(649\)](https://doi.org/10.1061/(ASCE)0733-9429(2007)133:6(649))
- van Rijn, L. C. (2007b). Unified view of sediment transport by currents and waves. II: Suspended transport. *Journal of Hydraulic Engineering*, 133(6), 668–689. [https://doi.org/10.1061/\(ASCE\)0733-9429\(2007\)133:6\(668\)](https://doi.org/10.1061/(ASCE)0733-9429(2007)133:6(668))
- Venditti, J. G., Dietrich, W. E., Nelson, P. A., Wyzdga, M. A., Fadde, J., & Sklar, L. (2010a). Effect of sediment pulse grain size on sediment transport rates and bed mobility in gravel bed rivers. *Journal of Geophysical Research*, 115, F03039. <https://doi.org/10.1029/2009jf001418>
- Venditti, J. G., Dietrich, W. E., Nelson, P. A., Wyzdga, M. A., Fadde, J., & Sklar, L. (2010b). Mobilization of coarse surface layers in gravel-bedded rivers by finer gravel bed load. *Water Resources Research*, 46, W07506. <https://doi.org/10.1029/2009wr008329>
- Wheaton, J. M., Brasington, J., Darby, S. E., & Sear, D. A. (2010). Accounting for uncertainty in DEMs from repeat topographic surveys: Improved sediment budgets. *Earth Surface Processes and Landforms*, 35. <https://doi.org/10.1002/esp.1886>
- Wilcock, P. R., Kenworthy, S. T., & Crowe, J. C. (2001). Experimental study of the transport of mixed sand and gravel. *Water Resources Research*, 37(12), 3349–3358. <https://doi.org/10.1029/2001wr000683>
- Wooster, J. K., Dusterhoff, S. R., Cui, Y., Sklar, L. S., Dietrich, W. E., & Malko, M. (2008). Sediment supply and relative size distribution effects on fine sediment infiltration into immobile gravels. *Water Resources Research*, 44, W03424. <https://doi.org/10.1029/2006WR005815>
- Wren, D. G., Langendoen, E. J., & Kuhnle, R. A. (2011). Effects of sand addition on turbulent flow over an immobile gravel bed. *Journal of Geophysical Research*, 116, F01018. <https://doi.org/10.1029/2010JF001859>
- Wu, F.-C., & Chou, Y.-J. (2003). Simulation of gravel-sand bed response to flushing flows using a two-fraction entrainment approach: Model development and flume experiment. *Water Resources Research*, 39(8), 1211. <https://doi.org/10.1029/2003WR002184>
- Zimmermann, A. E., & Lapointe, M. (2005). Intergranular flow velocity through salmonid redds: Sensitivity to fines infiltration from low intensity sediment transport events. *River Research and Applications*, 21(8), 865–881. <https://doi.org/10.1002/rra.856>